ASCAT Soil Moisture Report Series No. 15

ASCAT Soil Moisture Product Handbook

Vienna University of Technology
Institute of Photogrammetry and Remote Sensing

2008 November 11

How to reference this report:

> Bartalis, Z., Naeimi, V., Hasenauer, S., Wagner, W. (2008). *ASCAT Soil Moisture Product Handbook.* ASCAT Soil Moisture Report Series, No. 15, Institute of Photogrammetry and Remote Sensing, Vienna University of Technology, Austria.

Contact Information:

Institute of Photogrammetry and Remote Sensing (I.P.F.)
Remote Sensing Group (Prof. Wagner)
Vienna University of Technology
Gusshausstrasse 27-29/E122
1040 Vienna, Austria

mbox@ipf.tuwien.ac.at
www.ipf.tuwien.ac.at

<table>
<tr><td>Status:</td><td colspan="3">Issue 1.3</td></tr>
<tr><td>Authors:</td><td colspan="3">IPF TU Wien (ZB)</td></tr>
<tr><td>Circulation:</td><td colspan="3">IPF, EUMETSAT</td></tr>
<tr><td>Amendments:</td><td colspan="3"></td></tr>
<tr><th>Issue</th><th>Date</th><th>Details</th><th>Editor</th></tr>
<tr><td>Issue 1.0</td><td>2008 Nov 11</td><td>Initial Document.</td><td>ZB</td></tr>
<tr><td>Issue 1.1</td><td>2008 Nov 26</td><td>After BUFR compliance of flags</td><td>ZB</td></tr>
<tr><td>Issue 1.2</td><td>2008 Nov 30</td><td>After comments from WW</td><td>ZB</td></tr>
<tr><td>Issue 1.3</td><td>2008 Dec 05</td><td>After comments from JF/EUM (Also changed “Product Guide” to “Product Handbook”, to avoid confusion.)</td><td>ZB</td></tr>
</table>

If further corrections are required please contact Zoltan Bartalis (zb@ipf.tuwien.ac.at).

List of Acronyms

AMI	Active Microwave Instrument (onboard ERS)
ASCAT	Advanced Scatterometer
BUFR	Binary Universal Form for the Representation of meteorological data (WMO)
ECMWF	European Centre for Medium-Range Weather Forecasts
ERA-40	ECMWF Reanalysis
EPS	EUMETSAT Polar System
ERS	European Remote Sensing Satellite
EUMETSAT	European Organisation for the Exploitation of Meteorological Satellites
DGG	Discrete Global Grid
GEM6	Goddard Earth Model 6
GLWD	Global Lakes and Wetlands Database
GRACE	Gravity Recovery and Climate Experiment
KNMI	Koninklijk Nederlands Meteorologisch Instituut (Royal Netherlands Meteorological Institute)
MDR	Main Data Record
NRT	Near-Real Time
OSI SAF	Ocean and Sea Ice Satellite Application Facility
PPF	Product Processing Facility
RD	Reference Document
SSM/I	Special Sensor Microwave/Imager
TU WIEN	Vienna University of Technology
U-MARF	Unified Meteorological Archive and Retrieval Facility (EUMETSAT)
WARP	Water Retrieval Package
$\mathrm{WARP}^{\mathrm{NRT}}$	Water Retrieval Package for Near-Real Time
WMO	World Meteorological Organization

Reference Documents

EUMETSAT Documents

RD1 ASCAT Products Guide, ref. EUM/OPS/-EPS/MAN/04/0028, available at http://oiswww.eumetsat.org/WEBOPS/eps-pg/ASCAT/ASCAT-PG-index.htm.

IPF/TU Wien Documents

RD2 Discrete Global Grid Systems, ASCAT Soil Moisture Report Series No. 4, available at http://www.ipf.tuwien.ac.at/radar/ascat/report_series/04_Discrete%20Global%20Grid%20Systems_2.2.pdf.

Journal and Conference Proceedings Articles, Other Documentation

Attema, E. P. W. (1991). "The Active Microwave Instrument On-Board the ERS-1 Satellite." Proceedings of the IEEE **79**(6): 791-799.

Attema, E. P. W. and F. T. Ulaby (1978). "Vegetation Modeled as a Water Cloud." Radio Science **13**: 375.

Bartalis, Z., R. A. Kidd and K. Scipal (2006a). Development and implementation of a discrete global grid system for soil moisture retrieval using the MetOp ASCAT scatterometer. First EPS/MetOp RAO Workshop, 15-17 May 2006, Frascati, Italy, ESA Special Publication SP-618.

Bartalis, Z., K. Scipal, V. Naeimi and W. Wagner (2004). Soil moisture products from C-band scatterometers: From ERS-1/2 to METOP. ENVISAT-ERS Symposium, Salzburg, Austria, 6-10 September.

Bartalis, Z., K. Scipal and W. Wagner (2006b). "Azimuthal anisotropy of scatterometer measurements over land." IEEE Transactions on Geoscience and Remote Sensing **44**(8): 2083-2092.

Bartalis, Z., W. Wagner, V. Naeimi, S. Hasenauer, K. Scipal, H. Bonekamp, J. Figa and C. Anderson (2007). "Initial soil moisture retrievals from the METOP-A Advanced Scatterometer (ASCAT)." Geophysical Research Letters **34**(L20401).

Ceballos, A., K. Scipal, W. Wagner and J. Martínez-Fernández (2005). "Validation of ERS scatterometer-derived soil moisture data in the central part of the Duero Basin, Spain." Hydrological Processes **19**(8): 1549-1566.

de Jeu, R., W. Wagner, T. Holmes and H. Dolman (2008). "Global soil moisture patterns observed by space borne microwave radiometers and scatterometers." Surveys in Geophysics: DOI 10.1007/s10712-008-9044-0.

de Lange, R., R. Beck, N. van de Giesen, J. Friesen, A. de Wit and W. Wagner (2008). "Scatterometer derived soil moisture calibrated for soil texture with a one-dimensional water flow model." IEEE Transactions on Geoscience and Remote Sensing: in press.

Dirmeyer, P. A., Z. C. Guo and X. Gao (2004). "Comparison, validation, and transferability of eight multiyear global soil wetness products." Journal of Hydrometeorology **5**(6): 1011-1033.

Figa-Saldaña, J., J. J. W. Wilson, E. Attema, R. Gelsthorpe, M. R. Drinkwater and A. Stoffelen (2002). "The advanced scatterometer (ASCAT) on the meteorological operational (MetOp) platform: A follow on for European wind scatterometers." Canadian Journal of Remote Sensing **28**(3): 404-412.

Fontaine, B., S. Louvet and P. Roucou (2007). "Fluctuations in annual cycles and inter-seasonal memory in West Africa: rainfall, soil moisture and heat fluxes." Theoretical and Applied Climatology **88**(1-2): 57-70.

Fung, A. K. (1994). Microwave Scattering and Emission Models and Their Applications. Norwood, MA, USA, Artech House.

Hillel, D. (2003). Introduction to Environmental Soil Physics, Academic Press.

Kottek, M., J. Grieser, C. Beck, B. Rudolf and F. Rubel (2006). "World map of the Koppen-Geiger climate classification updated." Meteorologische Zeitschrift **15**: 259-263.

Künzer, C., D. Zhao, K. Scipal, D. Sabel, S. Hasenauer and W. Wagner (2008). "El Niño influences represented in ERS Scatterometer derived soil moisture data." Applied Geography: in press.

Lecomte, P. (1998). The ERS scatterometer instrument and the on-ground processing of its data. Emerging Scatterometer Application Workshop, ESTEC, Noordwijk, The Netherlands.

Lehner, B. and P. Döll (2004). "Development and validation of a global database of lakes, reservoirs and wetlands." Journal of Hydrology **296**: 1-22.

Naeimi, V., Z. Bartalis and W. Wagner (2008a). "ASCAT Soil Moisture: An Assessment of the Data Quality and Consistency with the ERS Scatterometer Heritage." IEEE Transactions on Geoscience and Remote Sensing **in press**.

Naeimi, V., C. Kuenzer, S. Hasenauer, Z. Bartalis and W. Wagner (2007). Evaluation of the influence of land cover on the noise level of ERS-scatterometer backscatter. IEEE International Geoscience and Remote Sensing Symposium, Barcelona, Spain, 23-28 July.

Naeimi, V., K. Scipal, Z. Bartalis, S. Hasenauer and W. Wagner (2008b). "An Improved Soil Moisture Retrieval Algorithm for ERS and Metop Scatterometer Observations." IEEE Transactions on Geoscience and Remote Sensing: in press.

Pellarin, T., J.-C. Calvet and W. Wagner (2006). "Evaluation of ERS scatterometer soil moisture products over a half-degree region in southwestern France." Geophysical Research Letters **33**(17): Art. No. L17401, doi:10.1029/2006GL027231.

Rüdiger, C., T. Holmes, J.-C. Calvet, R. d. Jeu and W. Wagner (2008). "An intercomparision of ERS-Scat, AMSR-E and SVAT soil moisture observations over France." Journal Of Hydrometeorology: in press, doi:10.1175/2008JHM997.1.

Scipal, K., M. Drusch and W. Wagner (2008). "Assimilation of a ERS scatterometer derived soil moisture index in the ECMWF numerical weather prediction system." Advances in Water Resources **31**: 1101-1112.

Scipal, K., C. Scheffler and W. Wagner (2005). "Soil moisture-runoff relation at the catchment scale as observed with coarse resolution microwave remote sensing." Hydrology and Earth System Sciences **9**(3): 173-183.

Taconet, O., D. Vidal-Majar, C. Emblanch and M. Normand (1996). "Taking into account vegetation effects to estimate soil moisture from C-band radar measurements." Remote Sensing of Environment **56**: 52-56.

Ulaby, F. T., R. K. Moore and A. K. Fung (1982). Microwave Remote Sensing: Active and Passive. Volume 2: Radar Remote Sensing and Surface Scattering and Emission Theory. Reading, Massachusetts, Addison-Wesley, Advanced Book Program.

Wagner, W. (1998). Soil Moisture Retrieval from ERS Scatterometer Data. Vienna, Austria, Vienna University of Technology.

Wagner, W., G. Lemoine, M. Borgeaud and H. Rott (1999a). "A study of vegetation cover effects on ERS scatterometer data." IEEE Transactions on Geoscience and Remote Sensing **37**(2II): 938-948.

Wagner, W., G. Lemoine and H. Rott (1999b). "A method for estimating soil moisture from ERS scatterometer and soil data." Remote Sensing of Environment **70**(2): 191-207.

Wagner, W., J. Noll, M. Borgeaud and H. Rott (1999c). "Monitoring soil moisture over the Canadian Prairies with the ERS scatterometer." IEEE Transactions on Geoscience and Remote Sensing **37**: 206-216.

Wagner, W. and K. Scipal (2000). "Large-scale soil moisture mapping in western Africa using the ERS scatterometer." IEEE Transactions of Geoscience and Remote Sensing **38**(4): 1777-1782.

Wagner, W., K. Scipal, C. Pathe, D. Gerten, W. Lucht and B. Rudolf (2003). "Evaluation of the agreement between the first global remotely sensed soil moisture data with model and precipitation data." Journal of Geophysical Research D: Atmospheres **108**(D19): Art. No. 4611.

Wahr, J., S. Swenson, V. Zlotnicki and I. Velicogna (2004). "Time-variable gravity from GRACE: First results." Geophysical Research Letters **31**: L11501, doi:10.1029/2004GL019779.

Contents

1 Introduction

The present document is the product handbook of the soil moisture part of the ASCAT Level 2 product disseminated by EUMETSAT. It is intended to serve as a guide and quick reference for users of the ASCAT soil moisture product, and complements Reference Document RD1.

The ASCAT soil moisture product is produced by EUMETSAT, using the so-called WARP^{NRT} software originally developed by IPF/TU Wien (Institute of Photogrammetry and Remote Sensing, Vienna University of Technology) and prototyped for EUMETSAT. ASCAT soil moisture is delivered in orbit geometry as part of the ASCAT Level 2 product, in two different spatial resolutions: 50 km (25 km grid spacing) and approximately 25 km (12.5 km grid spacing). For the dissemination data formats and timeliness, see Section 6.2 in RD1.

Section 2 below gives a brief description of the ERS and ASCAT scatterometers. Section 3 summarises the scientific background of the soil moisture retrieval and its implementation, for both the long-term scattering parameter database, as well as well as the ASCAT product derived in a NRT regime. Section 4 presents the different fields of the ASCAT soil moisture product output and describes the relevant data structures for the cases of two distribution formats: EPS (EUMETSAT native file format for EUMETSAT Polar System products), and WMO BUFR.

This document was prepared under the EUMETSAT contract EUM/CO/05/1412/HGB.

2 The ERS and ASCAT Scatterometers

Scatterometers are microwave sensors designed to measure the normalized radar cross section (sigma-nought, σ^0) with high radiometric accuracy over a set of different incidence and azimuth angles (θ and φ, respectively). They have the advantage of providing day- and night-time measurements unaffected by cloud cover. Spaceborne scatterometers are used to measure surface properties with relatively coarse spatial resolutions but on a relatively frequent basis.

2.1 The Scatterometer onboard ERS-1 and ERS-2

The scatterometer onboard the ERS-1 and ERS-2 satellites is part of the Active Microwave Instrument (AMI) consisting of a synthetic aperture radar and a fan beam scatterometer operating in C-band (5.6 GHz) at VV polarization. The three scatterometer antennae generate radar beams looking sideways with respect to the satellite flight direction, at 45° (fore), 90° (mid), and 135° (aft), and at incidence angles ranging from 18° to 59°. The three antenna beams continuously illuminate a 500 km wide swath, each measuring the radar backscatter for so-called cells, which for the Level 1 data are approximately 50 km wide and spaced at 25 km from each other. The result is three independent backscatter measurements (a σ^0 triplet) at the nodes of a 25 km swath grid, taken practically simultaneously and at different viewing angles (1991).

ERS-1 regularly acquired data between August 1991 and May 1996. ERS-2 operated nominally between March 1996 and January 2001, when due to a failure of a gyroscope all ERS-2 instruments were temporarily switched off. Since May 2004, reception of ERS-2 data is limited to selected regions (North America, Europe, Northwest Africa, China, Australia), as ERS-2 had lost its onboard data storage capability in June 2003. Fig. 3–1 shows the availability of measurements on a global scale from August 1991 to May 2007. In April 2007 the ERS-2 spacecraft reached its 12th year in orbit. Apart from some minor problems all platform subsystems and payload instruments are working satisfactorily and are providing high quality data. Recently, the ERS-2 mission was approved to be continued for three more years until 2011.

2.2 ASCAT onboard Metop

The advanced scatterometer (ASCAT), like its predecessor, the ERS scatterometers, uses a fan-beam antenna technology. In contrast to ERS, it uses two sets of three antennae, one on each side of the satellite ground track. For ASCAT the incidence angle range is extended to 25°–65°. ASCAT covers two 550 km swaths separated by approximately 360 km from the satellite ground track. The ASCAT instrument operating continuously as a scatterometer, its coverage is then approximately three times of that of the ERS scatterometers. ASCAT also features a number of technical improvements. The improved instrument design and radiometric performance result in higher σ^0 stability and reliability. In addition to the 50 km resolution, the Level 1B product is also delivered with approximately 35 km resolution (referred to as 25 km resolution product, since its orbit spacing is 12.5 km) (Figa-Saldaña et al. 2002).

3 The Soil Moisture Retrieval Method

The TU Wien method for retrieving soil moisture from ASCAT scatterometer data is, from its conception, a change detection method. The scientific basis and algorithms have been fully published in a series of conference and journal papers, most important of which are Wagner et al. (Wagner et al. 1999a; Wagner et al. 1999b; Wagner et al. 1999c), Wagner and Scipal (2000), Wagner et al. (2003), Naeimi et al. (2008a; 2008b).

In order to obtain ASCAT soil moisture values, instantaneous ASCAT backscatter measurements are extrapolated to a reference incidence angle (chosen to be 40°) and corrected for the seasonal influence of vegetation. This is done by exploiting the multi-incidence angle viewing capabilities of the ERS/ASCAT scatterometers. They are then compared to equivalent existing dry and wet ERS backscatter references ($\sigma^0{}_{dry}$ and $\sigma^0{}_{wet}$ respectively), also defined at 40°. As a result, time series of the topsoil (< 5 cm) moisture content m_s are obtained in relative units ranging between 0 (dry) and 100 (saturated).

For a better understanding of the ASCAT soil moisture product, knowledge about how $\sigma^0{}_{dry}$, $\sigma^0{}_{wet}$ and other long-term reference values are derived is needed. We will therefore first present a brief summary of the long-term global scattering parameter database created from ERS-1 and ERS-2 data and used for deriving the soil moisture product in NRT regime (Section 3.1). We will then present how the NRT ASCAT product is derived using the database (Section 3.2).

3.1 The Long-Term Reference Scattering Parameter Database

All global parameters required for the processing of scatterometer backscatter in NRT regime are stored in a long-term reference scattering parameter database. This database is quasi-static, i.e. it is intended to be updated roughly each 3–5 years, incorporating future ERS-2 and ASCAT data.

Presently, the database is based on merged ERS-1 and ERS-2 backscatter time series of the period August 1991 to May 2007 (for the majority of locations this period is August 1991 – January 2001, due to restricted coverage of the ERS-2 scatterometer after this date, see Section 2.1).

Computation of soil moisture parameters is established in IPF/TU Wien's so-called WARP software. The package allows a stepwise processing of Level 1 backscatter (spatially averaged σ^0 response) described in the following sections.

3.1.1 Step 1: Data resampling

The scatterometer data are rearranged from the orbit geometry to a time series format over a predefined discrete global grid (DGG). The grid is based on the GEM6 ellipsoid, also used for the ground range projection of ERS-1/2 and ASCAT data in orbit geometry (Lecomte 1998), and generated by an adapted partitioning of the globe with approximatively 12.5 km grid spacing. Details of the used DGG are found in Bartalis et al. (2006a) and RD2. For the present version of WARP, backscatter (σ^0), incidence angle (θ) and azimuth angle (φ) values from the same satellite overpass and antenna beam were resampled to the DGG using a Hamming weighting function of 36 km width, resulting in time series for each DGG point. Given the present 50 km resolution of the ERS data (25 km grid), an oversampling is implied. This is intentional, since the grid is defined to accommodate a future version of the ERS data, reprocessed to 25 km resolution. From this point on, the successive processing steps are applied to each of the time series separately. The number of available resampled ERS-1/2 σ^0 triplets is shown in Figure 3–1.

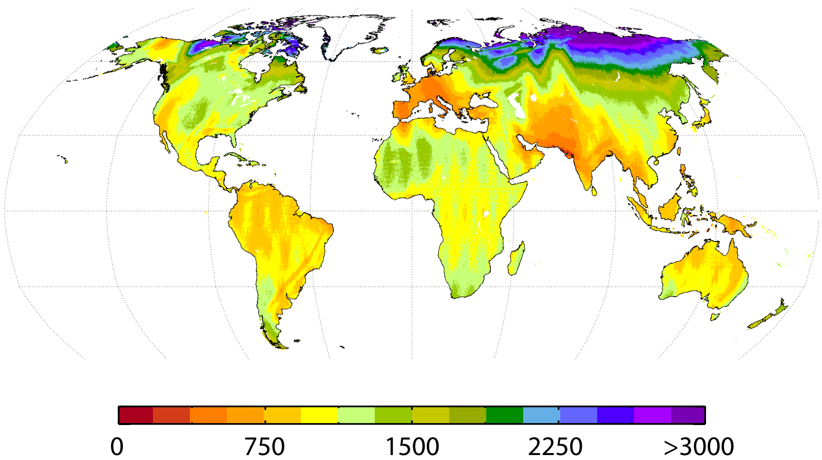

Figure 3–1

Number of the resampled SCAT measurements from August 1991 to May 2007.

3.1.2 Step 2: Azimuthal normalisation

Since for some regions backscatter varies significantly with azimuth angle (Bartalis et al. 2006b), σ^0 is normalised in terms of its acquisition φ: a correction bias is applied to the σ^0 values for each possible antenna azimuth (a discrete combination between beam type and ascending/descending track direction), using look-up tables. To calculate the biases, a second order polynomial is applied to model the σ^0 variations with respect to θ for each azimuth combination. The difference between these polynomials and the polynomial derived for the entire dataset is used as a correction bias.

3.1.3 Step 3: Estimated standard deviation of sigma-0

The Estimated Standard Deviation (ESD) of σ^0 due to instrument noise, speckle and residual azimuthal effects is computed, based on triplet-wise differences between the fore- and aft antenna beam σ^0 values:

$$ESD(\sigma^0) = \frac{StDev(\sigma^0_{fore} - \sigma^0_{aft})}{\sqrt{2}} \quad (3\text{–}1)$$

Figure 3–2 shows the resulting global ESD map.

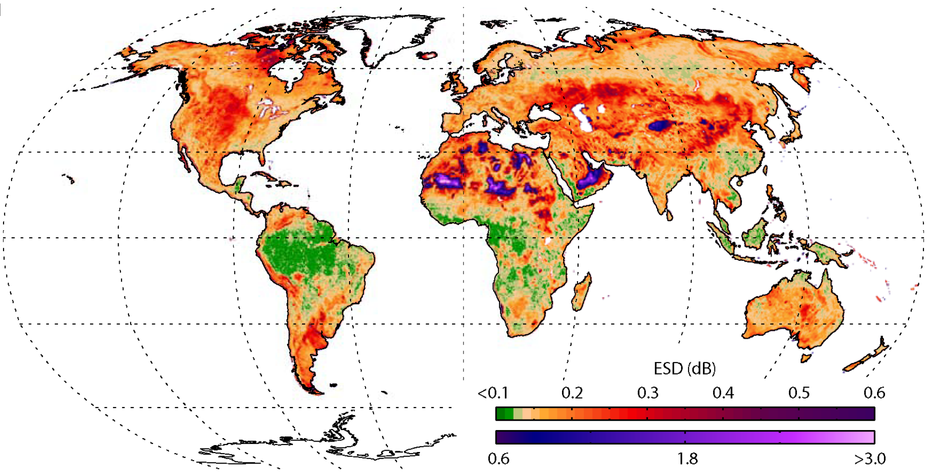

Figure 3–2

Estimated Standard Deviation of backscatter (ESD).

3.1.4 Step 4: Determining the yearly cycle of the derivatives of sigma-0 at 40° with respect to incidence angle

The σ^0 values collocated to each DGG point are measured at different incidence angles. As the intensity of backscatter signal strongly depends on the incidence angle θ, the σ^0 measurements cannot be compared directly and need to be normalised to a reference incidence angle. Therefore, all σ^0 measurements are extrapolated to the reference angle of 40° using a second order polynomial:

$$\sigma^0(40,t) = \sigma^0(\theta,t) - \sigma'(40,t)(\theta - 40) - \frac{1}{2}\sigma''(40,t)(\theta - 40)^2\,, \quad (3\text{–}2)$$

where σ' and σ'' are the first and, respectively, second derivatives of σ^0 with respect to θ. The reference angle is set to 40° in order to minimize extrapolation errors (Wagner et al. 1999b). The parameters of this model, the slope σ' and the curvature σ'', are determined from simultaneous multi-incidence angle observations:

$$\sigma'(\frac{\theta_{mid} - \theta_{fore/aft}}{2}) = \frac{\sigma^0_{mid}(\theta_{mid}) - \sigma^0_{fore/aft}(\theta_{fore/aft})}{\theta_{mid} - \theta_{fore/aft}} . \tag{3–3}$$

Having a large set of samples evenly distributed over the entire incidence angle range, $\sigma'(40)$ and $\sigma''(40)$ can be derived by fitting a linear model of the form

$$\sigma'(\theta) = \sigma'(40) + \sigma''(40)(\theta - 40) . \tag{3–4}$$

The exact shape of the polynomial expressed in Equation 3–2 depends on the land surface properties, such as the state of vegetation and the roughness of the surface. Less rough surfaces with little vegetation result in a steep decline of σ^0 with respect to θ and therefore low, negative $\sigma'(40)$ values. Increased vegetation and rough surfaces generally result in higher $\sigma'(40)$ values. Each of the slope and the curvature thus show a distinct annual cycle, determined by vegetation growth and decay. When determining these annual cycles, one needs to do a trade-off between a sensitive but noisy annual curve and a less-responsive but robust one. This is achieved by a method similar to a Monte Carlo simulation, where the final $\sigma'(40)$ and $\sigma''(40)$ values for each of the 366 days of the year are computed as the arithmetical average of many annual curves, each calculated with a time window ranging between 2 and 12 weeks. For each of the $\sigma'(40)$ and $\sigma''(40)$, the variability of the annual curve families will be a measure of the relative noise of $\sigma'(40)$ and $\sigma''(40)$, respectively.

The result of this processing step are thus sets of 366 values for each DGG point for each of the following variables: slope at 40°, curvature at 40°, noise of slope at 40°, noise of curvature at 40°.

3.1.5 Step 5: Calculating sigma-0 at 40° and its noise

Based on Equation 3–2 above, $\sigma^0(40)$ is calculated, as well as its noise, using error propagation on the noise values obtained in Section 3.1.4. The result is time series of $\sigma^0(40)$ and its associated noise, for each of the DGG points.

3.1.6 Step 6: Calculating the dry and wet backscatter references at 40°

The dominant mechanisms contributing to $\sigma^0(40)$ are volume scattering effects in the vegetation canopy and surface scattering from the underlying soil surface (Fung 1994). In simple radiative transfer models like the Cloud Model (Attema and Ulaby 1978), the effect of vegetation is largely controlled by the optical depth which weighs the relative contribution of surface and volume scattering. Although a different parameterization is used in WARP, its functionality is similar with these models. When vegetation grows, the optical depth increases, and the volume scattering term becomes more important. This does not necessarily mean that backscatter increases. In situations where the reduced contribution from the underlying ground is more important than the enhanced volume scattering, σ^0 decreases. For low incidence angles, the effect of vegetation is mainly attenuation of the signal returned by underlying soil (Taconet et al. 1996). In other words, backscattering from bare soil is in general stronger than vegetated soil in near range. Because of rapid drop-off of the bare soil backscatter the situation may be reversed at high incidence angles. Therefore, at some incidence angle, $\sigma^0(\theta)$ curves of a developing and a full grown vegetation canopy should cross over (Wagner 1998). In the TU Wien model it is assumed that the effect of vegetation is minimal at the so-called "crossover" angles θ_{dry} and θ_{wet}, which differ for dry and wet soil conditions. If such crossover angle exists then for dry conditions it should be found at lower incidence angles than for wet conditions (Wagner et al. 1999c).

The TU Wien model is essentially a change detection method relating $\sigma^0(40,t)$ to the lowest and highest values of $\sigma^0(40)$ ever recorded. The lowest and highest values are presumed to be references of the driest and the wettest conditions of soil surface. A significant step before determination of the dry/wet references is removing outliers in the $\sigma^0(40)$ time series. This should be done cautiously to avoid eliminating valid measurements. The outliers in the $\sigma^0(40)$ distribution are representing faulty data because of systematic errors like instrument malfunctioning or situations where the algorithm might not be valid. Such outliers are detected in two individual phases during the calculation of dry/wet references. In the first step, values greater than 3 interquartile distances from the mean are removed from the $\sigma^0(40)$ distribution. After separating extreme low and high values in the $\sigma^0(40)$ distribution, the outlier removal procedure is performed once again to remove outliers greater than 1.5 interquartile distances from the mean, in both groups of the extreme low and high observations.

The backscatter coefficients under dry and wet conditions are estimated by taking an average of the extreme lowest and highest measurements. In WARP, the extreme low values in $\sigma^0(\theta_{dry})$ and the extreme high values in $\sigma^0(\theta_{wet})$ distributions are separated with respect to an explicit uncertainty range, defined as a 95% 2-sided confidence interval of the measurements. The confidence interval of the extreme low and high values is obtained by considering the noise of $\sigma^0(\theta_{dry})$ and $\sigma^0(\theta_{wet})$:

$$\text{Confidence Interval} = \pm 1.96 \times (\text{Noise of } \sigma^0(\theta)) \tag{3–5}$$

The value 1.96 represents the 97.5 percentile of the standard normal distribution, which is often rounded to 2 for simplicity. Consequently, the mean values of the separated extreme observations are considered as dry and wet references at the presumed crossover angles:

$$C^0_{dry} = \frac{1}{N_{lower}} \sum_{i=1}^{N_{lowet}} \sigma^0_i(\theta_{dry}), \tag{3–6}$$

$$C^0_{wet} = \frac{1}{N_{upper}} \sum_{i=1}^{N_{upper}} \sigma^0_i(\theta_{wet}), \tag{3–7}$$

where N_{lower} and N_{upper} are the number of low and high extreme values in the $\sigma^0(\theta_{dry})$ and $\sigma^0(\theta_{wet})$ distributions respectively.

Knowing C^0_{dry} and C^0_{wet} and considering Equation 3–2, dry and wet references at 40° are obtained as

$$\begin{aligned}\sigma^0_{dry}(40,t) = C^0_{dry} &- \sigma'(40,t)(\theta_{dry} - 40) \\ &- \frac{1}{2}\sigma''(40,t)(\theta_{dry} - 40)^2\end{aligned} \tag{3–8}$$

and

$$\begin{aligned}\sigma^0_{wet}(40,t) = C^0_{wet} &- \sigma'(40,t)(\theta_{wet} - 40) \\ &- \frac{1}{2}\sigma''(40,t)(\theta_{wet} - 40)^2.\end{aligned} \tag{3–9}$$

As the crossover angles are set to $\theta_{wet} = 40°$ and $\theta_{dry} = 25°$ empirically, $\sigma^0_{dry}(40,t)$ describes an annual cycle while $\sigma^0_{wet}(40,t)$ will be constant.

In the course of the algorithm development it has become clear that in some arid regions the obtained $\sigma^0_{wet}(40)$ is too low due to the lack of captured saturated conditions during the entire observation period. As a temporary solution for dealing with such cases, an empirical bias-correction factor based on sensitivity is applied to $\sigma^0_{wet}(40)$. The locations for which this wet correction is applied are determined by using an external climatology dataset (Kottek et al. 2006). The magnitude of the applied bias is chosen so that the sensitivity (defined by convention as the difference $\sigma^0_{wet} - \sigma^0_{dry}$) in these areas increases to at least 5 dB. Figure 3–3 shows the sensitivity after the wet correction.

To conclude, after this processing step, sets of 366 values for each DGG point and for each of the following two variables are stored: the dry reference $\sigma^0_{dry}(40)$ and the wet reference $\sigma^0_{wet}(40)$ (for the present implementation constant in time and bias-corrected where needed). From these, the sensitivity can be calculated on the fly as $\sigma^0_{wet}(40) - \sigma^0_{dry}(40)$.

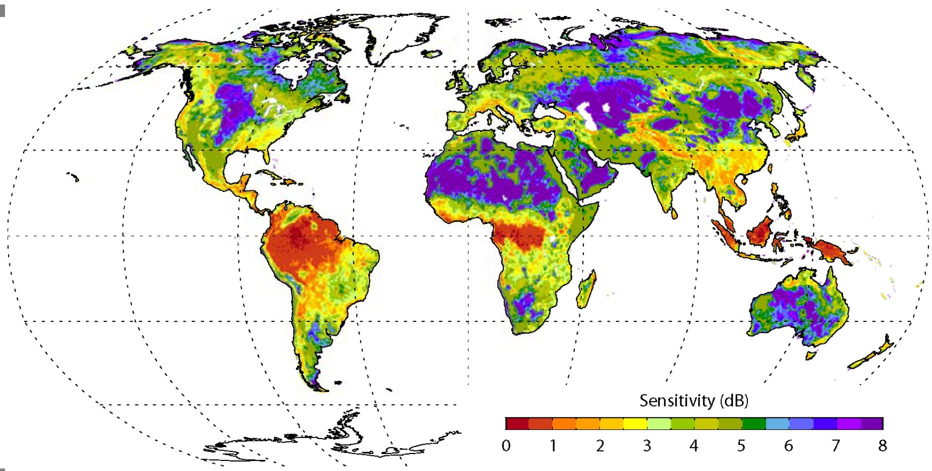

Figure 3–3
Sensitivity ($\sigma^0_{wet} - \sigma^0_{dry}$).

3.1.7 Step 7: Calculating the surface soil moisture and its long-term mean

The dry and (bias corrected) wet references derived in 3–8 and 3–9 are now used to determine the relative surface soil moisture content. This assumes a linear relationship between $\sigma^0(40)$ expressed in decibels and the surface soil moisture content (Ulaby et al. 1982), the relative soil moisture content in the surface layer is calculated as

$$\Theta_s(t) = \frac{\sigma^0(40,t) - \sigma^0_{dry}(40,t)}{\sigma^0_{wet}(40,t) - \sigma^0_{dry}(40,t)} \quad (3\text{–}10)$$

$\Theta_s(t)$ is a relative measure of the water content in the surface layer ranging between zero and one (0–100%). Assuming that σ^0_{dry} represents a completely dry and σ^0_{wet} a saturated soil surface, $\Theta_s(t)$ is equal to the degree of saturation, i.e. the soil moisture content expressed in percent of porosity (Hillel 2003). Along with the $\Theta_s(t)$ time series for each DGG, equivalent noise estimate time series are also calculated, based on error propagation. Figure 3–4 shows the yearly average of this noise estimate. Finally, daily long-term average $\Theta_s(t)$ values are also calculated (366 values for each DGG), by using a moving average window of 30 days width over data from all available years.

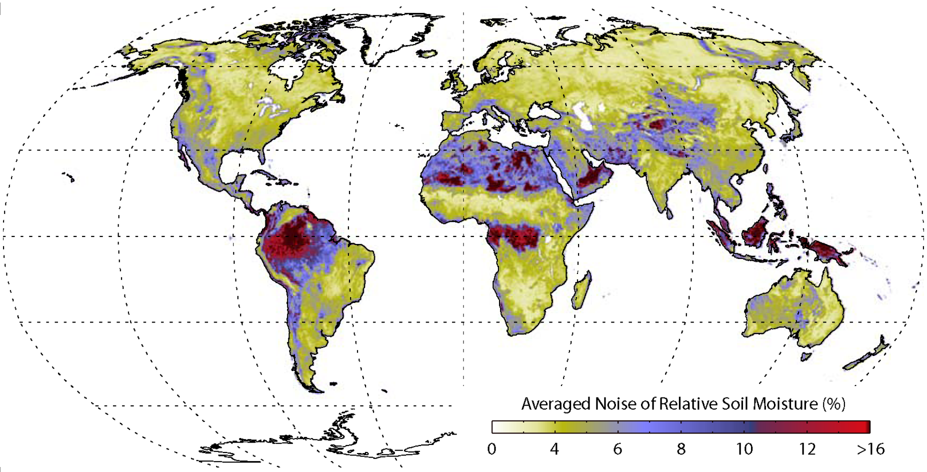

Figure 3–4

Average of the estimated soil moisture noise.

3.2 ASCAT Soil Moisture Retrieval in NRT Regime

Using the long-time global scattering parameter database from Section 3.1 above, the NRT product based on ASCAT backscatter as input is derived. NRT processing as implemented in WARP$^{\mathrm{NRT}}$ is in principle identical to the processing architecture of WARP, with the difference that required parameters are obtained by spatially interpolating the equivalent variables in the scattering parameter database, thereby making the processing quick and robust.

Additionally, advisory flags are added to the product, serving as data reliability indicators for the user. Some of these are currently derived from climatological data (See Section 4.2).

The processing steps involved in the creation of the ASCAT soil moisture product in NRT regime are as follows:

- Resampling the required variables from Section 3.1 to the ASCAT swath grid. For achieving this, a Hamming weighting function with radius 18 km is applied to the various parameters (constant and time-dependent) at each ASCAT swath grid location, always requiring a minimum of 3 DGG points with valid parameters.

- Reading the ASCAT Level 1B backscatter data and screening it according to the quality flags provided in the Level 1B product. Because of the currently different absolute σ^0 calibration between ERS and ASCAT scatterometers, and due to the fact that the soil moisture scatterometer parameter database has been derived from ERS data, ASCAT σ^0 values currently need to be applied a bias correction prior to running the soil moisture retrieval (see RD1).

- Normalising the σ^0 values with respect to their acquisition azimuth angles, using look-up tables derived in Section 3.1.2.

- Application of the algorithms to retrieve the surface soil moisture. Additional variables such as the normalised backscattering coefficient at 40° incidence angle, $\sigma^0(40)$, and its estimated noise, the estimated noise of the surface soil moisture, etc. are also calculated.

- Setting of so-called processing flags: whenever a processing flag is set, the soil moisture product could not be calculated, due to failing one or more quality checks of processing conditions. See the relevant field description in Section 4.1.7.

- Setting of so-called correction flags: whenever a correction flag is set, the soil moisture product is calculated, subject to some special restrictions (soil moisture values below 0% or above 100%, etc., see the relevant field description in Section 4.1.8.

- Setting of climatological advisory flags related to the probability of snow cover and frozen soil. Setting of advisory flags related to terrain topography, occurrence of wetlands. Calculating the long-term surface soil moisture mean.

The abovementioned processing steps are shown schematically in Figure 3–5.

3.3 Underlying Assumptions

The ASCAT soil moisture product is based on the following main assumptions:

- At the resolution of the scatterometer, roughness and land cover are temporal invariant. The measurement process suppresses local fluctuations of these parameters, due to the relatively high homogeneity of these measurables within the scatterometer footprint.
- Vegetation phenology influences on σ^0 are identical from year to year.
- There exist distinct incidence angles θ_{dry} and θ_{wet}, where the backscattering coefficient σ^0 is relatively stable despite seasonal changes in above ground vegetation biomass for dry and wet conditions, respectively.
- The relationship between soil moisture and σ^0, expressed in dB, is linear.

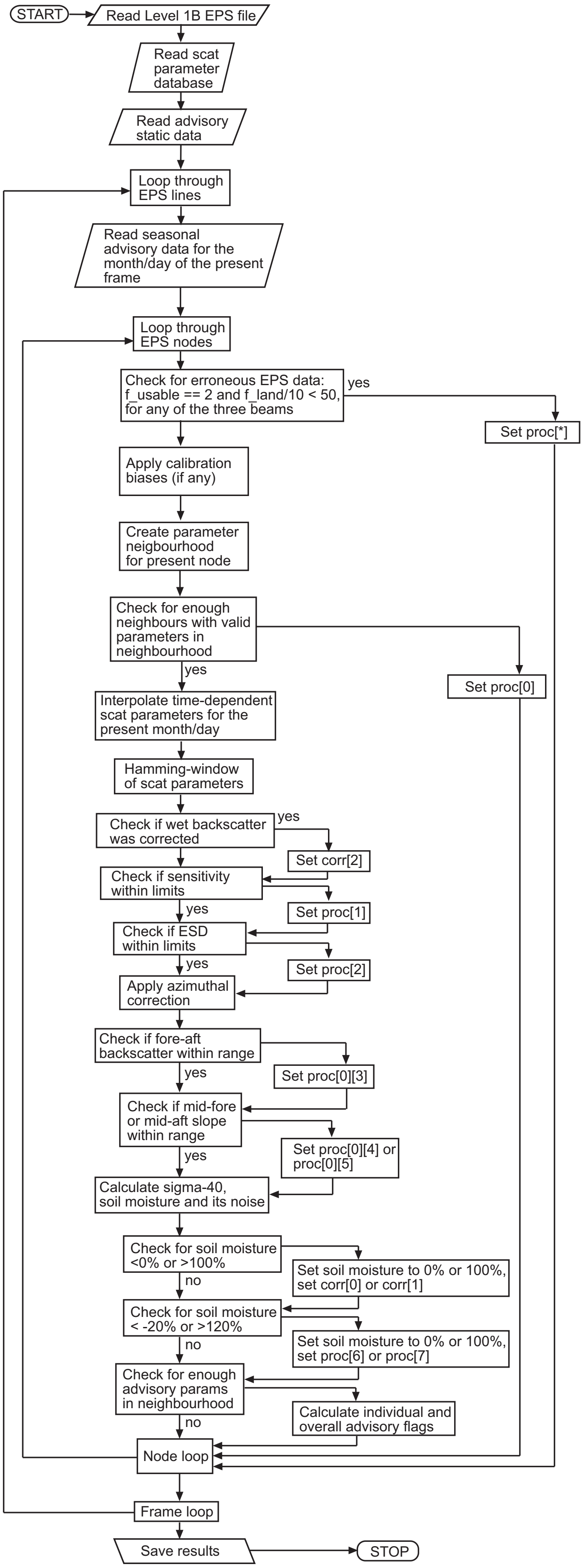

Figure 3–5

Flowchart of the ASCAT NRT soil moisture product processing steps.

4 ASCAT Soil Moisture Product Description

The ASCAT soil moisture product includes a number of parameters, which will briefly be discussed here.

4.1 Scatterometer-Based Output Variables

4.1.1 Surface soil moisture and its noise

The surface soil moisture measure represents the degree of saturation of the topmost soil layer (< 5 cm) and is given in percent, ranging from 0 (dry) to 100 (wet). This is equivalent to the processing step described in Section 3.1.7.

In extreme cases, the extrapolated backscatter at 40 degrees incidence angle may exceed the dry or the wet backscatter reference. In these cases, the value provided by the measurement process of surface soil moisture is, respectively, less than 0% or more than 100%. When this happens, the values are artificially set to 0% and 100% respectively. At the same time, the relevant correction flags (bits 1 and 2) are set.

An example of a visualisation of 50 and 25 km resolution surface soil moisture is shown in Figure 4–1.

The surface soil moisture is complemented by its noise, derived by error propagation of the backscatter noise (covering instrument noise, speckle and residual azimuthal effects). This is equivalent to the processing step described in Section 3.1.7.

4.1.2 Sigma-0 at 40° and its noise

For each input ASCAT σ^0 triplet, the equivalent σ^0 normalised to the reference incidence angle of 40° is calculated, using Equation 3–2 and slope and curvature values (first and second derivatives of the backscatter vs. incidence angle relationship) interpolated from the parameter database for the day of the year when the ASCAT triplet was acquired. The normalised backscatter is complemented by its noise, derived by error propagation of the backscatter noise (covering instrument noise, speckle and azimuthal effects). These values are equivalent to the of parameter database values derived in Section 3.1.5.

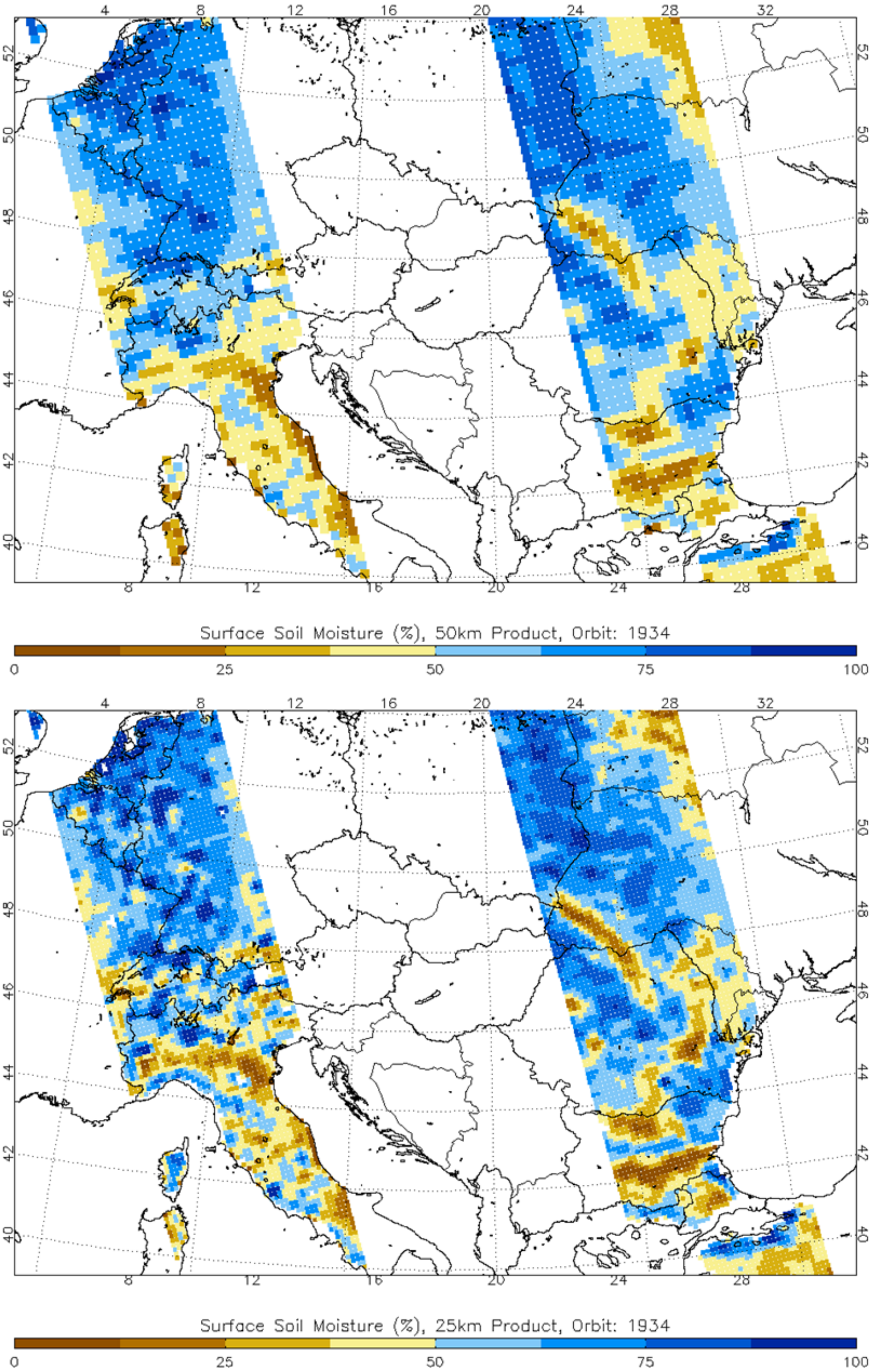

Figure 4–1

Examples of ASCAT surface soil moisture product with 50 km (top) and 25 km resolution (bottom) for February 2007.

4.1.3 Slope at 40° and its noise

These values are spatially interpolated from the equivalent parameter database values described in Section 3.1.4, for the day of the year when the ASCAT σ^0 triplet was acquired.

4.1.4 Sensitivity, dry backscatter reference, wet backscatter reference

These values are spatially interpolated from the equivalent parameter database values described in Section 3.1.6, for the day of the year when the ASCAT σ^0 triplet was acquired.

4.1.5 Long-term mean surface soil moisture

These values are spatially interpolated from the long-term average $\Theta_s(t)$ values calculated in Section 3.1.7, for the day of the year when the ASCAT σ^0 triplet was acquired.

4.1.6 Rainfall detection

Surface soil moisture is very sensitive to rainfall events. In principle, simple change detection should allow to track rainfall events in the surface soil moisture product. Currently a suitable method has not been implemented but given the importance of rainfall information in various applications, this flag has been reserved for future use.

4.1.7 Processing flags

A bit is set when it has value 1 and not set when it has value 0. All 16 bits set means that at least one beam of the ASCAT σ^0 input triplet is either of bad quality, according to the quality flags provided in the Level 1B product (the ASCAT Level 1B `f_usable` field is neither 0 or 1, see RD1) and/or the triplet is acquired over an area which is less than 50% land (see the `f_land` field in RD1).

- *Bit 1 set:* Not meaningful soil measurement since a) less than 3 valid neighbours in the parameter neighbourhood for Hamming windowing exist or b) the number of invalid neighbours is larger than the number of valid neighbours.
- *Bit 2 set:* Sensitivity to soil moisture below the 1 dB threshold. Soil moisture is nevertheless calculated.
- *Bit 3 set:* Azimuthal noise above limit, i.e. *ESD* (the estimated standard deviation from Section 3.1.3) is larger than the 1 dB threshold. Soil moisture is nevertheless calculated.

- *Bit 4 set:* Backscatter Fore-Aft beam out of range, i.e. $| \sigma^0_{fore} - \sigma^0_{aft} | > (6 * ESD)$ [in dB], where ESD is the estimated standard deviation from Section 3.1.3. Soil moisture is nevertheless calculated.
- *Bit 5 set:* The backscatter vs. incidence angle slope of the mid-fore beam measurement pair is out of range, i.e. larger than 6 times the noise of the slope from Section 3.1.4. Soil moisture is nevertheless calculated.
- *Bit 6 set:* The backscatter vs. incidence angle slope of the mid-aft beam measurement pair is out of range, i.e. larger than 6 times the noise of the slope from Section 3.1.4. Soil moisture is nevertheless calculated.
- *Bit 7 set:* Original soil moisture below -20%, value delivered, but set to 0% artificially.
- *Bit 8 set:* Original soil moisture above 120%, value delivered, but set to 100% artificially.
- *Bit 9-16:* Reserved for future use.

4.1.8 Correction flags

The bit flags of this one-byte value represent indications that although the soil moisture has been calculated, various restrictions in the data interpretation and usage apply. A bit is set when it has value 1 and not set when it has value 0.

- *Bit1 set:* Original soil moisture larger than or equal to -20% but less than 0%, value set to 0% artificially.
- *Bit2 set:* Original soil moisture larger than 100% but less than or equal to 120%, value set to 100% artificially.
- *Bit3 set:* Correction of wet backscatter reference applied.
- *Bit4 set:* Correction of dry backscatter reference applied. (currently not implemented).
- *Bit5 set*: Correction of volume scattering in sand applied. (Currently not implemented.)
- *Bit6-8*: Reserved for future use.

4.2 Non-Scatterometer-Based Output Variables

Soil moisture cannot be estimated if the fraction of dense vegetation, open water surfaces and/or snow/frozen soils dominates the scatterometer footprint. To support data users in judging the quality of the soil moisture products, advisory flags are stored as complementary information. Some of these flags are currently based on long-term climatologies (snow cover, frozen land surface) and *do not* represent exact conditions at the time of the soil moisture acquisition.

4.2.1 Snow cover fraction

Backscatter measurements are very sensitive to snow properties. The exact scattering behaviour of snow depends on the dielectric properties of the ice particles and on their distribution and density. Therefore soil moisture cannot be retrieved under snow conditions. The implementation of the snow flag uses a historic analysis of SSM/I (Special Sensor Microwave/Imager) snow cover data and gives the probability for the occurrence of snow for any day of the year. Examples of snow cover probabilities are given in Figures 4–2 and 4–3.

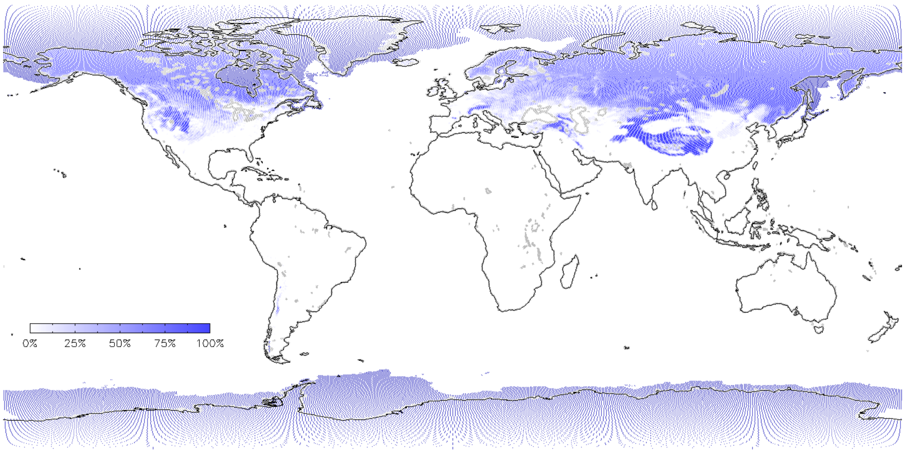

Figure 4–2

Snow Cover (derived using SSM/I) for the 1st of January.

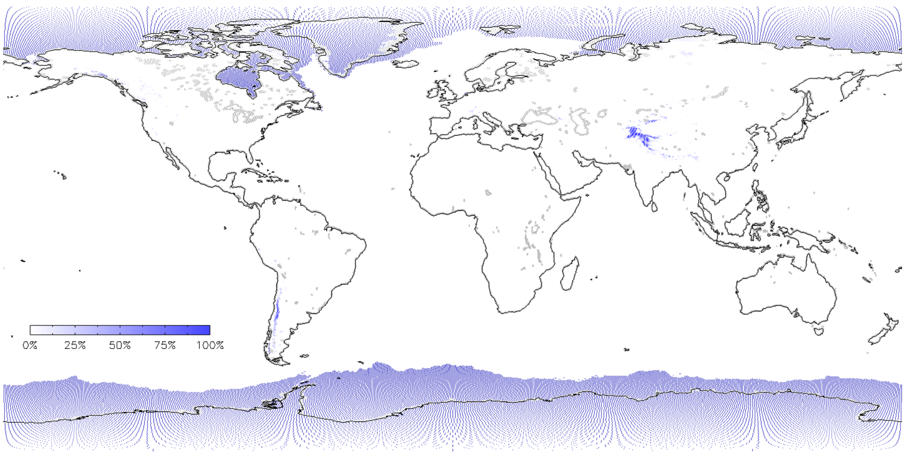

Figure 4–3

Snow Cover (derived using SSM/I) for the 1st of July.

4.2.2 Frozen land surface fraction

Taking into consideration the processes mentioned for snow, freezing can result in low backscatter, but also in high backscatter e.g. over frozen lakes. To avoid any negative implication in the use of backscatter representing frozen conditions these measurements have to be masked. The flag is based on a historic analysis of modelled climate data

(ECMWF ERA-40) and gives the probability for the frozen soil/canopy conditions for each day of the year (Figures 4–4 and 4–5).

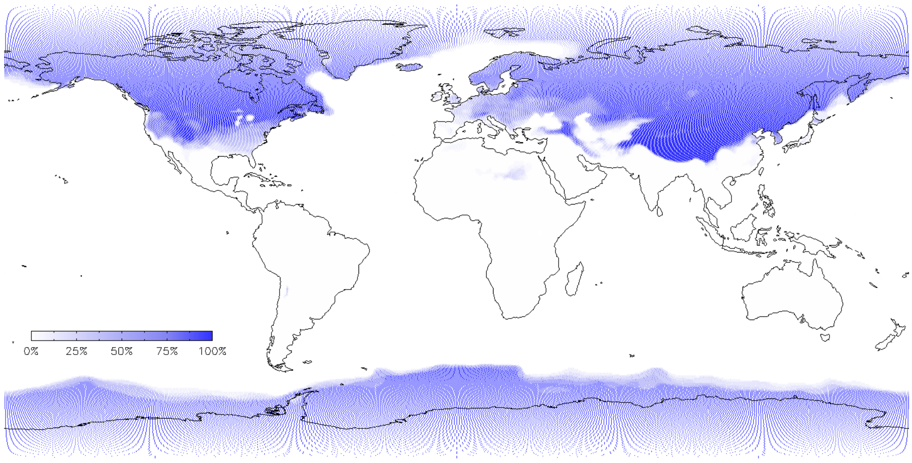

Figure 4–4

Frozen soil probability (ERA-40 modelled product) for January 1st.

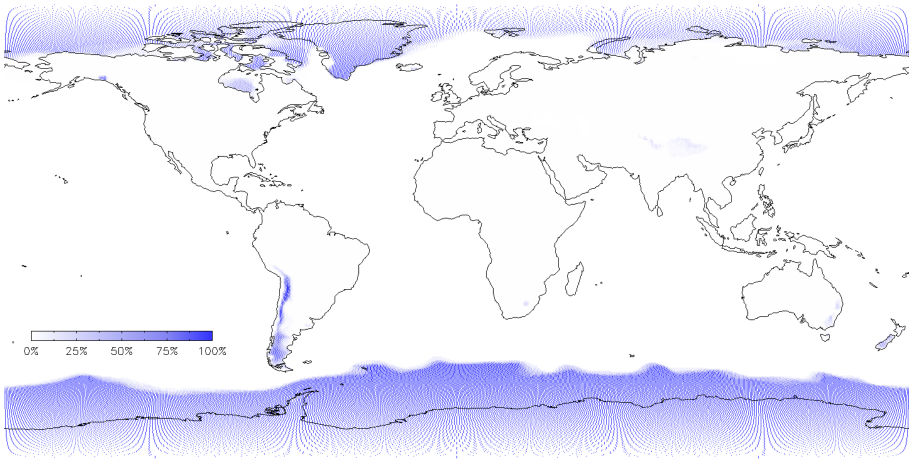

Figure 4–5

Frozen soil probability (ERA-40 modelled product) for July 1st.

4.2.3 Inundation and wetland fraction

The penetration depth of C-band microwaves into water is less than about 2 mm and therefore, as is the case for bare soil and wet snow, σ^0 of water is dependent on the roughness of the surface. When the water surface is calm, so-called specular reflection occurs and σ^0 at off-nadir angles is very low. Wind generates water waves that increase scattering into the backward direction. The radar return is highest when the radar looks into the upwind or downwind direction and is smallest when it looks perpendicularly to the wind direction. The main contributions do not come from large waves, even if they are many meters in height. Rather, scattering is dominated by short waves developing on the top of the larger waves. Generally, open water should not affect the soil moisture retrieval, if its area is small compared to the scatterometer footprint area. Nevertheless, there exist regions were the area percentage of open water surfaces can reach a significant magnitude, result in contamination of the evaluated soil moisture values.

To account for this, the open water flag is defined as fraction coverage of inundated and wetland areas. These areas are derived from the Global Lakes and Wetlands Database (GLWD) Level 3 product which includes several wetland and inundation types. An example of the inundation and wetland fraction is given in Figure 4–6.

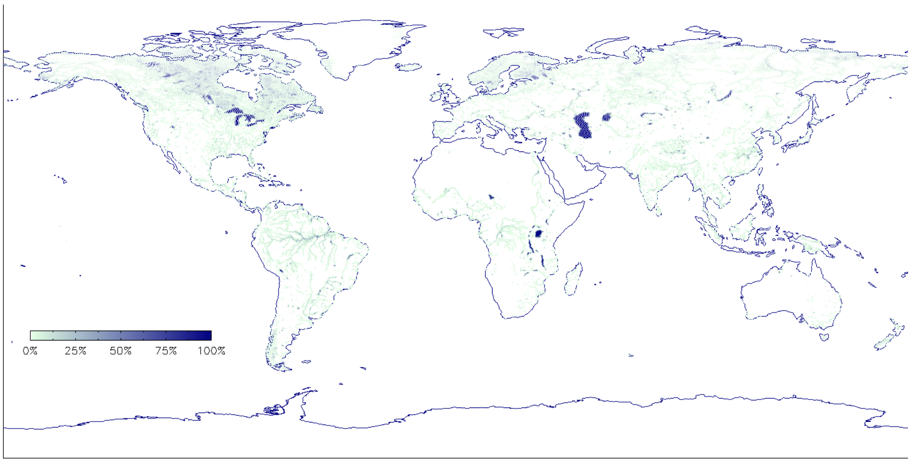

Figure 4–6

Inundation and wetland fraction derived from GLWD.

4.2.4 Topographic complexity

Backscatter of mountainous regions can be subject of several distortions. Main error sources are calibration errors due to the deviation of the surface from the assumed ellipsoid and the rough terrain, the influence of permanent snow and ice cover, a reduced sensitivity due to forest and rock cover and highly variable surface conditions.

The topographic complexity flag is derived from GTOPO30 data. For each cell of the DGG, the standard deviation of elevation is calculated and the result is normalized to values between 0 and 100 %, as can be seen in Figure 4–7.

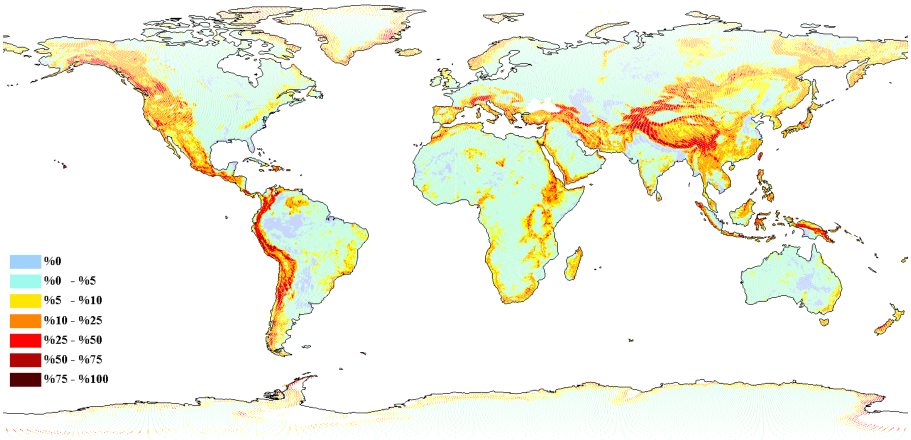

Figure 4–7

Topographic Complexity (Normalized standard deviation of topography), derived from GTOPO30.

4.2.5 Soil moisture quality

This is an aggregated quality control indicator serving as an overall quality flag. It is equal to the maximum value of the four advisory flags described above.

4.3 Product Validation

The quality of the ERS-based soil moisture (generated within the long-term parameter database) has been investigated following several strategies, ranging from comparison with precipitation data to comparison with modelled data or in-situ soil moisture data. Various studies showed that this dataset (and especially more refined profile soil moisture datasets derived from it) reflects trends in precipitation (Wagner et al. 2003; Fontaine et al. 2007), modelled soil moisture (Dirmeyer et al. 2004; Lehner and Döll 2004; Pellarin et al. 2006; de Jeu et al. 2008; Rüdiger et al. 2008), in situ soil moisture observations (Ceballos et al. 2005), and runoff (Scipal et al. 2005; de Lange et al. 2008). The dataset is also complementary to the series of GRACE (Gravity Recovery and Climate Experiment) gravitational observations related to the dynamics of the continental water storage (Wahr et al. 2004). It was also successfully assimilated into a numerical weather prediction system (Scipal et al. 2008). The dataset was even found to display El Niño effects (Künzer et al. 2008). A noise modelling of ERS soil moisture was carried out by Naeimi (2007) and Naeimi et al. (2008a). The noise estimates in these studies is only applicable for the 50 km product. Error estimates for the 25 km resolution product are expected to be higher by a constant factor, to be determined in future studies.

Given the very similar design of ERS and ASCAT scatterometers, the high consistency between the ERS and ASCAT products and the superior coverage and performance of ASCAT, the transition from ERS to ASCAT is expected to be smooth (Bartalis et al. 2004; Naeimi et al. 2008a) and we can be confident that the ERS results are equally valid for ASCAT. Investigations using ASCAT surface soil moisture have so far concentrated on case studies of extreme rainfall and drought events (Bartalis et al. 2007), showing promising results.